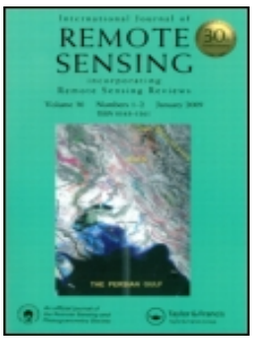

International Journal of Remote Sensing

ISSN: 0143-1161 (Print) 1366-5901 (Online) Journal homepage: https://www.tandfonline.com/loi/tres20

Semi-annual cycle of sea-surface temperature in the East/Japan Sea and cooling process

Kyung-Ae Park & Eun-Young Lee

To cite this article: Kyung-Ae Park & Eun-Young Lee (2014) Semi-annual cycle of sea-surface temperature in the East/Japan Sea and cooling process, International Journal of Remote Sensing, 35:11-12, 4287-4314, DOI: 10.1080/01431161.2014.916437

To link to this article: https://doi.org/10.1080/01431161.2014.916437

Published online: 28 May 2014.

International Journal of Remote Sensing, 2014
Vol. 35, Nos. 11–12, 4287–4314, http://dx.doi.org/10.1080/01431161.2014.916437

Taylor & Francis
Taylor & Francis Group

Semi-annual cycle of sea-surface temperature in the East/Japan Sea and cooling process

Kyung-Ae Park[a,b]* and Eun-Young Lee[c]

[a]*Department of Earth Science Education, Seoul National University, Seoul, Republic of Korea;*
[b]*Research Institute of Oceanography, Seoul National University, Seoul, Republic of Korea;*
[c]*Department of Science Education, Seoul National University, Seoul, Republic of Korea*

(*Received 22 July 2013; accepted 9 December 2013*)

Semi-annual cycles of the sea-surface temperature (SST) in the East/Japan Sea (EJS) and their forcings were examined by analysing National Oceanic and Atmospheric Administration/Advanced Very-High-Resolution Radiometer data, scatterometer wind vectors, and heat flux data. The semi-annual cycle contributed to the total variance of the SST by 8% and amounted to 25% of the amplitudes of the annual SST cycle, particularly in the Tatarskiy Strait and along the continental shelf off Russia. The lowest phase, corresponding to the minimum SST, occurred during early November and 6 months earlier in May or June depending on the position. The forcings of the semi-annual cycle were not semi-annual but substantially annual with a lag of 6 months, which gave rise to SST cooling in spring and autumn. Our analyses illustrated that SST cooling in autumn was caused by direct, local atmospheric wind forcings, whereas the cooling with large amplitudes of the semi-annual cycle in spring was caused by the non-local, remotely forced cold water advection of the Liman Current associated with sea-ice melting in the Tatarskiy Strait. The phase lag of 1–2 months between the complete melting of the sea ice in the Tatarskiy Strait and the surface cooling along the Russian continental shelf was related to the advection of cold water from sea ice in the form of the Liman Cold Current. The semi-annual cycle also resulted from asymmetry of the time series of the SST due to a long cold winter and a short warm summer. To understand how SST curves are distorted and asymmetric, we suggested two mathematical parameters of kurtosis and skewness. In addition, we suggest that the ratio of the semi-annual amplitude to the annual amplitude of SST harmonics can be used as a typical indicator of the asymmetry in year-to-year SST variations.

1. Introduction

The East/Japan Sea (EJS) is a small semi-enclosed marginal sea in the northwest Pacific, but its oceanic phenomena and circulation are quite similar to those of the open ocean (Ichiye 1984; Kim et al. 2001). Its bottom topography is characterized by deep basins (the Japan Basin, the Ulleung Basin, and the Yamato Basin) and a shallow region of the Yamato Rise in its central part (Figure 1). In the southern part of the EJS, there are the East Korea Warm Current (EKWC) along the east coast of Korea, the near-shore branch (NB) of the Tsushima Warm Current (TWC) along the Japanese coast, and its offshore branch (OB) between the EKWC and NB of the TWC, as shown in Figure 1 (Kawabe 1982; Yoon 1982). Prevailing cold currents in the northern part are the Liman Cold Current (LCC) flowing southwestward from the Tatarskiy Strait along the Russian coast

*Corresponding author. Email: kapark@snu.ac.kr

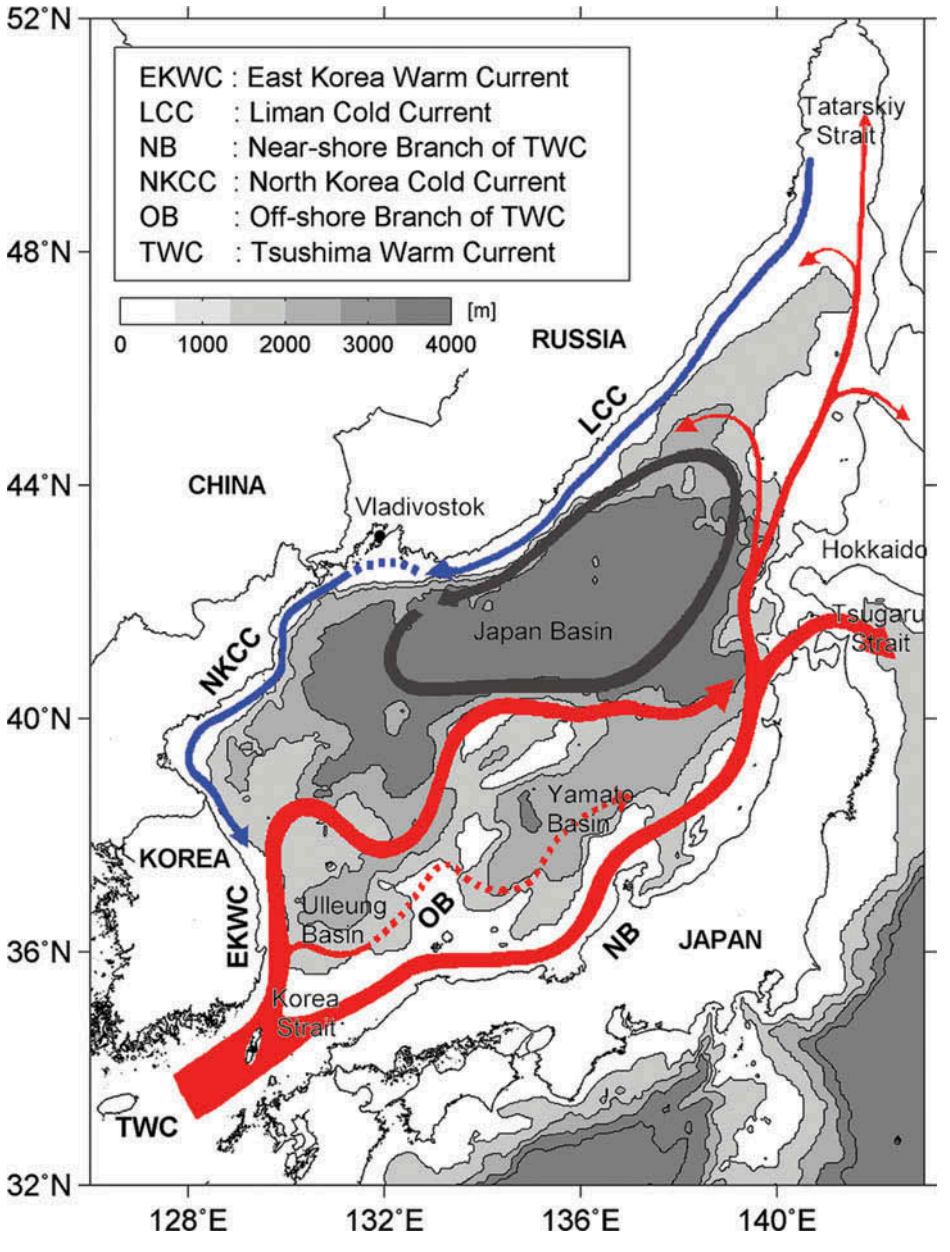

Figure 1. Bathymetry and the major currents in the East/Japan Sea. Abbreviations are in the upper left. The warm and cold currents are from Park et al. (2013).

and the North Korea Cold Current (NKCC) along the coast of North Korea that intermittently appears at the east coast of Korea (Park et al. 2013). Similar to the open ocean, the sub-polar front (SPF) is well developed along about 40° N between the warm and the cold waters in the central part of the EJS (Park, Chung, and Kim 2004).

Atmospheric conditions over the EJS vary widely from a subtropical climate in summer to a subarctic climate due to severe cold-air outbreaks in winter (Dorman et al.

2004). Diverse atmospheric forcings, such as surface heat flux, momentum flux, or wind stress forcing, control the spatial and temporal variability of the sea surface temperature (SST) in the EJS (Chu, Chen, and Lu 1998; Chen et al. 2001; Dorman et al. 2004; Minobe, Sako, and Nakamura 2004; Park et al. 2005). In turn, the SST field and the SPF can have an effect on the atmospheric circulations over the EJS through air–sea interactions (Chen et al. 2001). Moreover, in the most northern part of the EJS, sea ice is generated in the Tatarskiy Strait by severe storms, contributing to the formation of a cold current such as the LCC (Martin, Munoz, and Drucker 1992; Martin and Kawase 1998; Park et al. 2006). The atmospheric forcings associated with the winter storms are known to induce a considerable oceanic response, which is responsible for sea-ice formation and deep-water formation (Martin, Munoz, and Drucker 1992; Kawamura and Wu 1998; Talley et al. 2003).

Changes in the forcing field can modify the regular seasonality of SST variations by generating intra-seasonal to year-to-year variations of SST anomalies. Such a change creates asymmetry in the time variation of SST at a given location with a long cold period and a short warm period (Van Loon 1967; Provost, Garcia, and Garcon 1992) and can generate the spatial distinction of SSTs as well as associated temporal variations, such as the semi-annual signal of the SST.

In the Antarctic Ocean, the semi-annual SST cycle is known to be associated with a real atmospheric forcing caused by semi-annual waves present in the southern hemisphere (Van Loon 1967). Semi-annual variation in the western tropical Pacific Ocean was explained not by local Ekman pumping but by the westward propagation of Rossby waves originating in the central tropical Pacific (Qu et al. 2008). The annual and semi-annual variations of the SST in the North Pacific Ocean were determined by a harmonic analysis by Wyrtki (1965), in which the EJS was not included due to a lack of data. Yashayaev and Zveryaev (2001) presented SST harmonics in the Pacific Ocean that included the semi-annual cycle, but they presented only a gross spatial distribution in the EJS at coarse spatial grids. Except for these studies, to date, researchers have not given much attention to the semi-annual SST signal in the EJS. The annual harmonics of the SST in the EJS and their relationship with wind forcings and bathymetry were presented by Park et al. (2005).

Both annual and semi-annual cycles substantially explain the fundamental seasonal characteristics of SST anomalies (SSTAs). Therefore, an investigation of the semi-annual SST cycle can provide a key to understand what controls SSTA and how the asymmetry of the SST curve is generated. What process generated the cooling of the SST variations in spring and autumn? The primary hypothesis of this study is that atmospheric forcing or oceanic condition induces changes in SST deviated from annual SST variations and then generates a semi-annual cycle of SSTs as asymmetry of SST variations. The cooling process during autumn is expected to be mainly related to wind fields, while it will be associated with sea-ice melting in the northern region of the EJS in spring.

In short, our hypothesis on the semi-annual cycle of SSTs was that the autumn cooling was caused by local, non-advective, direct atmospheric wind forcings, whereas the spring cooling stemmed from remote, advective cold currents generated from sea-ice melting in the Tatarskiy Strait. Thus, the main objectives of this study are (1) to present the spatial pattern of SST harmonics (amplitudes and phases) of the semi-annual cycle in the EJS, (2) to examine the contribution of different SST cooling processes in spring and autumn to the components of the semi-annual cycle, (3) to characterize the asymmetry of SST variations by statistical parameters, and (4) to understand the relation between year-to-year variations of SSTA and those of wind speed in the EJS.

2. Data and processing

2.1. Satellite and oceanic data

All available passes of National Oceanic and Atmospheric Administration (NOAA) polar orbiting satellites for the period 1990 to 1995 were acquired from the Seoul National University/Research Institute of Oceanography for the EJS. The SST was estimated using NOAA's split-window multi-channel SST (MCSST) algorithms (Walton et al. 1998). The SST composites at a resolution of 1.1 km were produced over each semi-month of about 15 days. For the investigation of the semi-annual cycle of SST variations for a longer period, we used the Level-4 Multi-sensor Ultra-high-Resolution SST (MURSST) of the National Aeronautics and Space Administration (NASA) at a spatial resolution of 1 km and at daily intervals over a decade from 2003 to 2012 (http://mur.jpl.nasa.gov).

The accuracy of satellite-derived SST for NOAA satellites in the study area has been reported to be less than 1°C: for instance 0.91°C (Park et al. 1994), 0.7–0.8°C (Park et al. 1999), 0.75–1.0°C (Park et al. 2011), 0.56–0.89°C (Park, Sakaida, and Kawamura 2008a, 2008b), and 0.6°C (Sakaida and Kawamura 1992a, 1992b). Seasonal biases as overestimation (underestimation) of SST in summer (winter) were eliminated using a regionally optimized algorithm (Park et al. 1999). MURSST has been reported to have an RMS error of less than 1°C (Chin, Vazquez, and Armstrong 2013).

To investigate whether the semi-annual cycle is associated with real atmospheric forcing, we used Quick Scatterometer (QuikSCAT) wind vectors and heat flux reanalysis data from the National Centers for Environmental Prediction/National Center for Atmospheric Research (NCEP/NCAR). To examine spatial differences in SST responses to local net heat flux, climatology data of the mixed-layer depth (MLD) in the EJS were obtained from the database (Monterey and Levitus 1997) based on World Ocean Atlas (WOA) 1994 with a spatial grid of 1° × 1°. Temperature and salinity data from WOA 2001 with 0.25° × 0.25° were used to investigate their monthly variations (http://www.nodc.noaa.gov/OC5/indprod.html).

2.2. Harmonic and empirical orthogonal function (EOF) analyses

In the harmonic analysis, an individual time (t) series of SSTs ($SST(t_n)$, $n = 1,\ldots, N$) is the sum of the temporal SST mean $\overline{(SST)(t)}$ and M possible harmonic constituents A_q and B_q for M specified frequencies. The series is defined as

$$SST(t_n) = \overline{SST(t)} + \Sigma_{q=1}^{M}\left(A_q \cos\left(2\pi f_q t_n\right) + B_q \sin\left(2\pi f_q t_n\right)\right) + SST_r(t_n), \tag{1}$$

where $\overline{SST(t)}$ is the mean value of the SST data, SST_r is the residual portion of the time series that may contain other types of harmonic constituents, and t_n is $n\Delta t$ (Emery and Thomson 1998). The harmonic constants are estimated as follows:

$$C_q = \left({A_q}^2 + {B_q}^2\right)^{1/2}, \tag{2}$$

$$\varphi_q = \tan^{-1}\left(\frac{B_q}{A_q}\right). \tag{3}$$

Here, C_q, f_q, and φ_q are the constant amplitude, frequency, and phase of the q-th constituent, respectively. We estimated both annual and semi-annual harmonics (1–2

cycles per year) to understand the characteristics of the semi-annual cycle of SST variations in the EJS. In the present study, the term 'annual cycle' refers to the SST cycle with a frequency of 1 year, and the term 'seasonal cycle' refers to SST variations with the sum of the harmonic frequencies from 1 to 4 cycles per year.

In general, SSTA at each spatial grid (i,j) and time (t) is obtained by subtracting SST climatology from the SST. However, here the term *SSTA* was obtained by removing the annual cycle with one cycle per year ($q = 1$) from the *SSTs* instead of the climatology data as follows:

$$SSTA(i,j,t) = SST(i,j,t) - \left[\overline{SST(i,j)} + C_q(i,j)\ \sin\left(2\pi f_q t + \varphi_q(i,j)\right)\right]. \tag{4}$$

The characteristics of the residual SST variations were investigated to understand the semi-annual cycle. To simplify and quantify the spatial and temporal variability of SST residuals, referred to as SSTA henceforth, SSTA were decomposed into their dominant modes using an EOF analysis (Kelly 1988; Lagerloef and Bernstein 1988).

2.3. Kurtosis and skewness

We analysed the characteristics of SST asymmetry with mathematical notations such as kurtosis and skewness. Kurtosis is a measure of whether the data are peaked or flat relative to a normal distribution (Joanes and Gill 1998). Data sets with high kurtosis tend to have a distinct peak near the mean, decline rather rapidly, and have heavy tails. By contrast, data sets with low kurtosis tend to have a flat top near the mean rather than a sharp peak. Skewness is a measure of symmetry, or more precisely, the lack of symmetry. Negative (positive) values for skewness indicate that the data are skewed left (right). Negative skewness implies that data has a long tail on the left relative to the right tail. Similarly, data skewed right with positive skewness has a longer right tail compared to the left tail.

The analyses of the statistical parameters use the same concept of kurtosis and skewness; however, the calculation methods were different. SST variations have a curve as a function of time. In order to estimate the degree of asymmetry quantitatively, we regarded the time series of the SSTs as the histogram of the SSTs and then estimated the two parameters based on fundamental mathematics.

2.4. Wavelet analysis

Fourier transform provides an average amplitude over the entire time series, whereas wavelet analysis has shown better performance for non-stationary signals (Meyers, Kelly, and O'Brien 1993; Liu and Miller 1996; Emery and Thomson 1998; Elsayed 2010). The variables such as SST, SSTA, wind, or sea-ice concentration in this study are all non-stationary data with high temporal variabilities from seasonal and year-to-year variations. To investigate the relationship between time-varying SST and other atmospheric-oceanic variables, we applied wavelet analysis to the satellite data. The continuous wavelet transform, X, of a real time series, $x(t)$, with respect to the analysing wavelet, $g(t)$, is defined through the convolution integral

$$X_g[\tau, a] = (1/\sqrt{a}) \int_{-\infty}^{\infty} g^*[a^{-1}(t-\tau)]x(t)\mathrm{d}t, \tag{5}$$

where g^* denotes the complex conjugate of g and variables τ, a are allowed to vary continuously through the domain (Emery and Thomson 1998). The wavelet analysis yields X_g as a measure of the localized amplitude a as the wavelet moves through the time series with increasing values of τ (Emery and Thomson 1998).

3. Results

3.1. Contribution of semi-annual cycle to total SST variance

The annual cycle of the SST in the EJS accounted for between 88% and 96% of the total variance, which was quite large compared to the central region of the North Pacific (84–88%) at similar latitudes (Yashayaev and Zveryaev 2001; Park, Chung, and Kim 2004). The semi-annual cycle contributed to the total variance of the SST by less than 12% (Figure 2). It showed a notable spatial distinction between the northern and southern areas of the EJS. General features of the semi-annual cycle were characterized by a dominant region in the northern region north of the SPF extending to 40° N. In particular, it makes a relatively large contribution to the total variance of the SST of as much as 6% in the Tatarskiy Strait and along the continental shelf off the Russian Primorye coast of about 4% (Figure 2(*a*)). By contrast, its contribution was very small, at less than 2%, in the southern EJS south of the SPF. Its contribution to the total variance is reduced to a minimum along the east coast of Korea.

The mean ratio of the semi-annual amplitude to the annual amplitude ranged from 5% to 35% (Figure 2(*b*)). North of the SPF, a relatively large fraction of about 22% appeared along the continental shelf off the Russian coast and a peak of about 30% appeared at the eastern area of the Tatarskiy Strait. The surface condition south of Vladivostok is known to be influenced by extreme cold-air outbreaks in winter (Dorman et al. 2004). Such predominant annual forcings generate a noticeable annual SST cycle and heat flux centre through air–sea heat exchanges in this region (Kawamura and Wu 1998; Park et al. 2005). In contrast, the semi-annual cycle in this region showed a relatively small fraction of about 18% of the total variance (Figure 2(*b*)) due to the dominant annual cycle with an amplitude of about 11°C south of Vladivostok (Park et al. 2005). In the area south of the SPF, the ratios are much smaller, at less than 14% compared to the ratio north of the SPF. Relatively small values of 6–12% appeared on the eastern coast of Korea, where the EKWC flows northward.

Recent changes in the SST from 2003 to 2012 also revealed a similar feature in terms of the variance of the semi-annual cycle and its ratio to the annual cycle (Figures 2(*c*) and (*d*)). Because the MURSST database was objectively interpolated from both high-resolution infrared and low-resolution microwave measurements, the spatial structures in Figures 2(*c*) and (*d*) appear to be somewhat monotonous compared to the result from the NOAA/Advanced Very-High-Resolution Radiometer data. Nevertheless, both SSTs presented typical features of the semi-annual cycle with a high degree of similarity.

3.2. Amplitude and phase of semi-annual cycle

Our previous study (Park et al. 2005) showed that the difference in the SST north and south of the SPF in the EJS amounted to 15°C in winter and 10°C in summer and large annual amplitudes ranging from 6°C to 11°C. In contrast, the amplitudes of the semi-annual cycle were relatively small, at less than 3°C, over the basin (Figure 3(*a*)). Regions

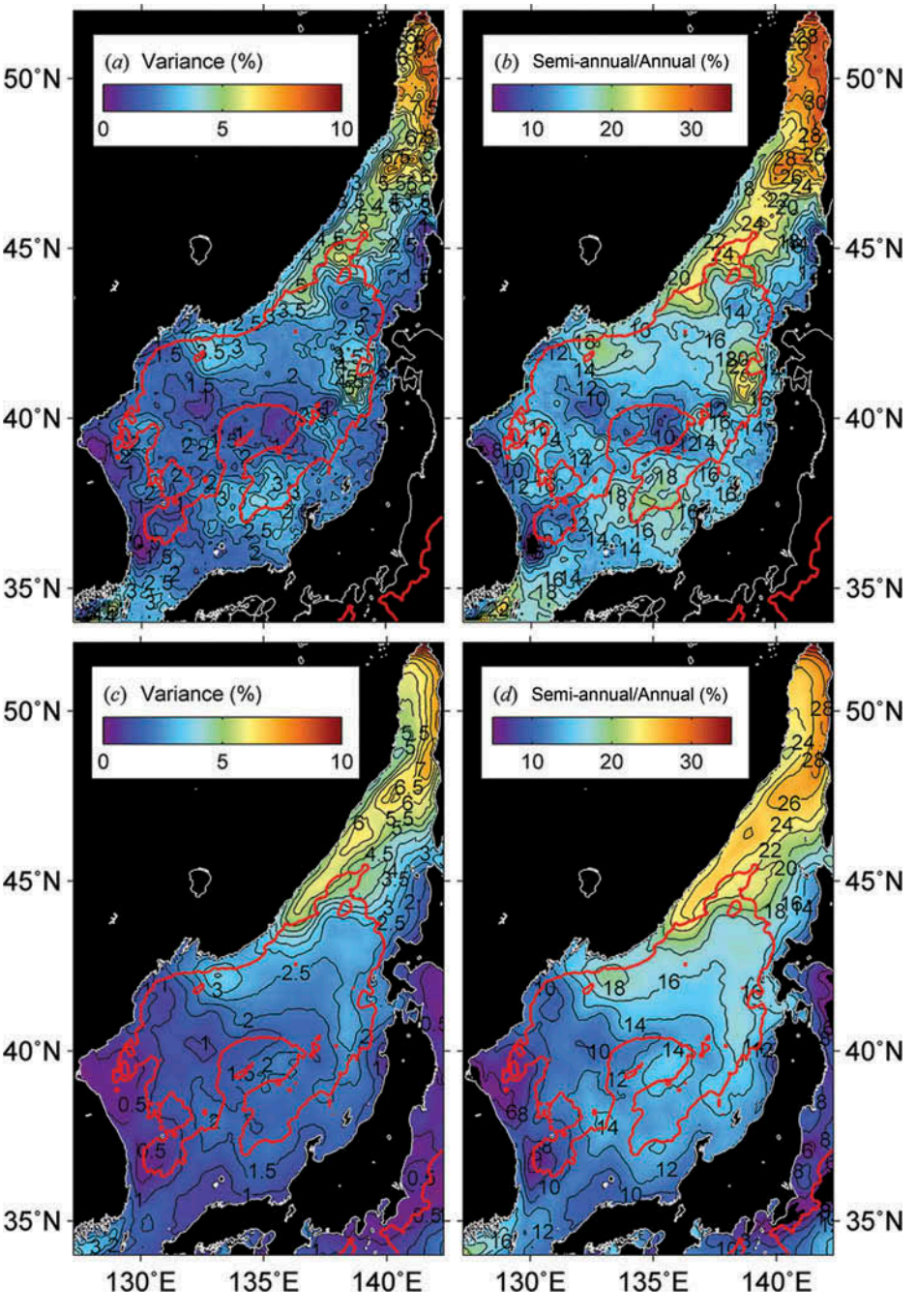

Figure 2. Spatial distribution of (*a*) contribution of semi-annual cycle to total variance of SST in the East/Japan Sea (%) and (*b*) the ratio of semi-annual amplitude to annual amplitude (%) for 6 years (1990–1995) and (*c*) and (*d*) are the results using recent 10 year SST data from 2003 to 2012. The red line represents a 2000 m contour of bottom topography.

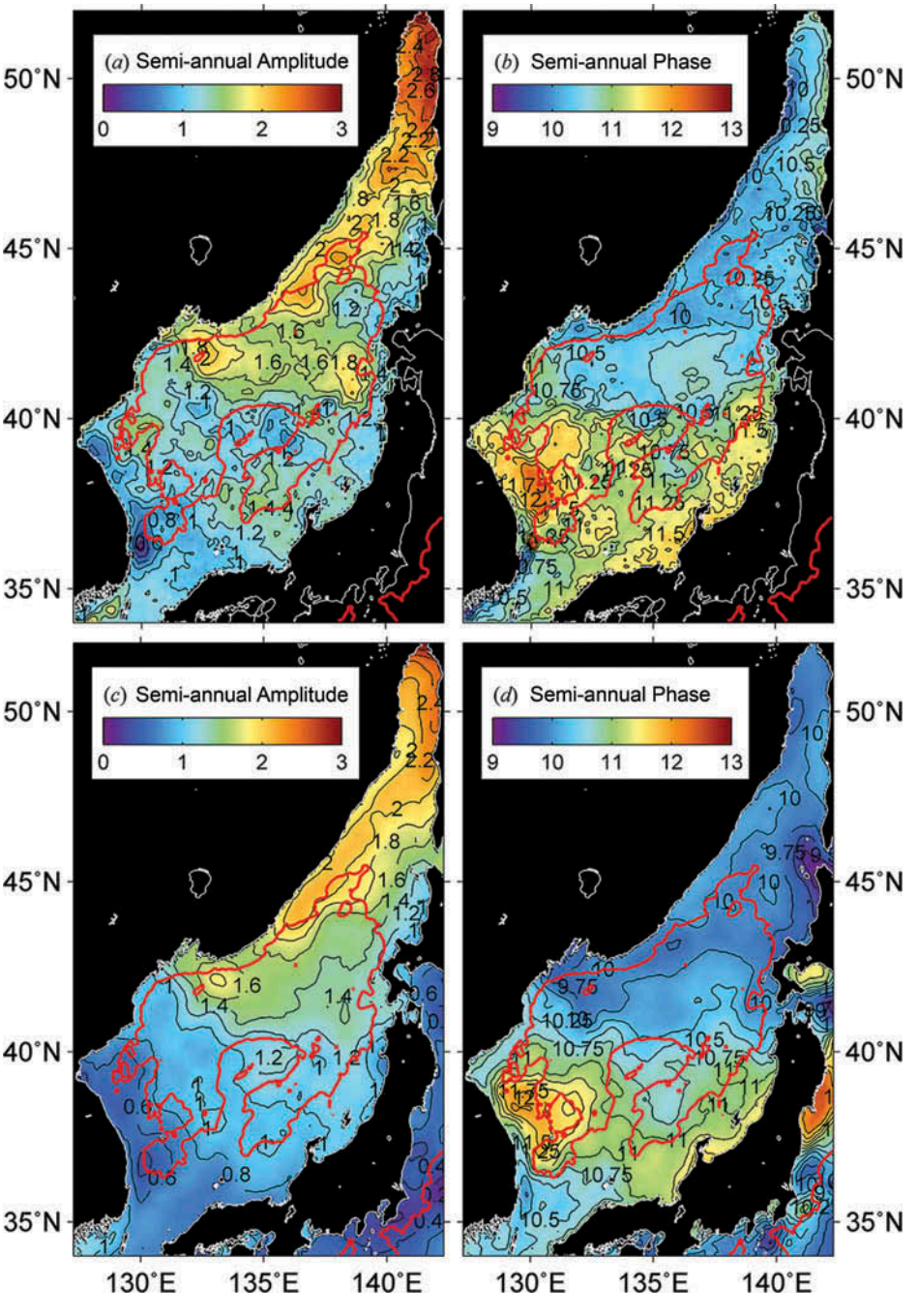

Figure 3. (*a*) Amplitude (°C) and (*b*) phase (decimal month) of semi-annual cycle of SST variations for the past 6 years (1990–1995) and (*c*) amplitude (°C) and (*d*) phase for the recent 10 year SST data from 2003 to 2012, where the phases were converted to a decimal month when the SST for semi-annual frequency reached a minimum in autumn. Superimposed red line is a 2000 m contour of bottom topography.

south of the SPF along 40° N showed small amplitudes of less than 1.4°C, whereas cold regions north of the SPF tended to have relatively large amplitudes of 1.6–3.0°C (Figure 3(*a*)). Particularly, large amplitudes of 2.0–3.0°C appeared in the Tatarskiy Strait and along the continental shelf off the Russian coast.

The phase of the semi-annual cycle at a given location was converted to a decimal month when it reached a minimum. Because it is the semi-annual cycle, the SSTAs have two minima of negative values per year. The phase information herein was selected for the time corresponding to autumn instead of spring. If the minima of SSTAs in autumn appear in mid-November, the phase month will be 10.5. Comparing Figures 3(*a*) and (*b*), it can be seen that majority regions north of the SPF showed values of less than 10.5, implying that the minimum of the semi-annual amplitudes in Figure 3(*a*) occurred before mid-November (Figure 3(*b*)). The Tatarskiy Strait and the Primorye off the Russian coast, with relatively high semi-annual amplitudes over 2°C, showed low phases of less than 10.25, corresponding to early November. The lowest phase of less than 10 in the western part of the Tatarskiy Strait implied that SSTs are damped down quickly, starting in late October. Strong cold winds from Siberia begin to blow from October over the sea surface in the Tatarskiy Strait (Park et al. 2003) and generate sea ice through heat loss from November to March in the following year (Martin and Kawase 1998). Strong cold winds from Siberia begin to blow from October over the sea surface in the Tatarskiy Strait (Park et al. 2003) and generate sea ice through heat loss from November to March in the following year (Martin and Kawase 1998). We will explore it in Section 3.5. Because the cycle period is 6 months, SST cooling is assumed to appear 6 months earlier, i.e. in early May, in most regions north of the SPF, as shown in Figure 3(*b*). South of the SPF, the semi-annual phase of around 11.25 was much later by 1 month than that north of the SPF. However, the phase information of the semi-annual cycle south of the SPF may be less significant than that north of the SPF because its contribution to the variance of the SST was minor, as shown in Figure 2(*a*).

The semi-annual cycle tended to intensify SST cooling from the annual variations of the SST in November and May and therefore increased the asymmetry of the SST curves. Thus, it is of interest to investigate whether the semi-annual cycle is related to real forcings with a 6 month period and to determine the processes that generate the spatial distinction in the semi-annual cycle. In the following sections, we examine the characteristics of SST cooling that produce the semi-annual cycle in a time series of the SST.

3.3. Dominant EOF mode of SSTA variations

To understand SSTA variations that deviate from the annual cycle, we decomposed the SSTA into the dominant EOF modes. Figure 4 presents the first EOF mode of SSTA and its time-varying amplitudes, which account for 55.97% of the variability in SSTA. Such spatial distributions show good agreement with the spatial pattern of variance and the amplitudes of the semi-annual cycle in Figures 2 and 3. The eigenvectors exhibited higher values that were greater than 6×10^{-3} in the regions north of 43° N, particularly the Tatarskiy Strait and the Primorye coast. By contrast, they were small, at about 2.5×10^{-3}, in the EKWC region ($<3 \times 10^{-3}$) (Figure 4(*a*)).

The time-varying amplitudes of the first EOF mode manifestly demonstrated two peaks per year (Figure 4(*b*)). The local minimum of each semi-annual cycle appeared in spring and late autumn per year, respectively. The amplitudes of the first EOF mode showed dominant year-to-year variations with a minimum of about –500 during the spring of 2011, of which the causes and mechanisms should be further studied. The time series of the amplitudes in

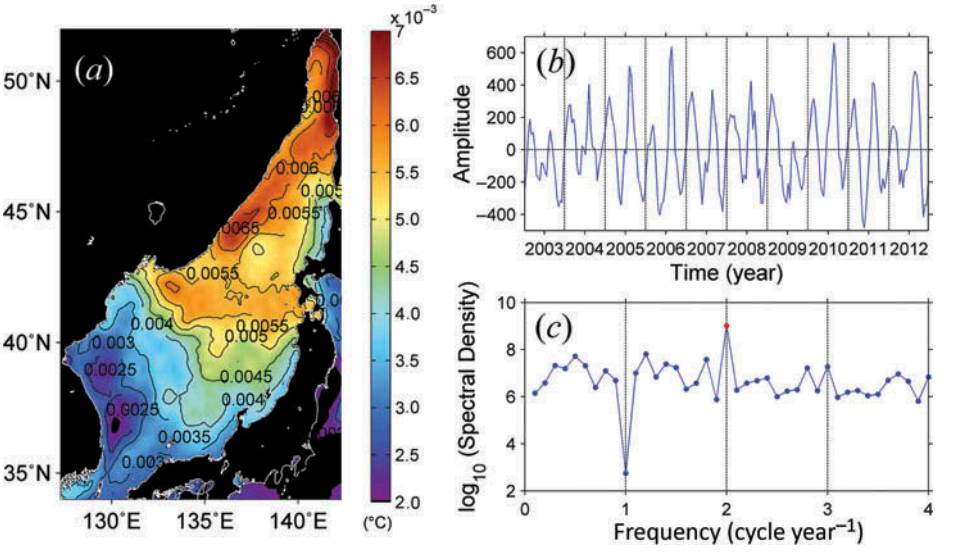

Figure 4. (*a*) Spatial distribution of eigenvectors from the first EOF mode using SSTA data in the East/Japan Sea, (*b*) time-varying amplitude of (*a*) for a recent decade from 2003 to 2012, and (*c*) the spectral density ($\log_{10}$) of the time-varying amplitudes in (*b*).

Figure 4(*b*) exhibit a dominant peak of the spectral density at a frequency of two cycles per year (Figure 4(*c*)). This spectral peak implied that the semi-annual cycle of SSTs consisted of major variations of SSTA apart from the annual cycle.

3.4. Characteristics of SSTA

The semi-annual signal was the most dominant component of SSTA, defined as the SST minus the annual cycle henceforth. The SSTA can explain the characteristics of the SST cooling process. Figure 5(*a*) shows the time series of the MURSST (black solid) and the fitted annual cycle (blue solid) averaged over an area of about 50 km× 50 km (46.975–47.475° N, 139.725–140.225° E) at the southern Tatarskiy Strait for the period of 2003–2012, for which the SSTAs (the SST minus the annual cycle) are plotted by the red line at the bottom of the plot. The time series of the SSTAs shows notable periodic oscillation corresponding to semi-annual frequency with amplitudes of about 5°C (Figure 5(*a*)). Two specific negative peaks twice a year were noted, in spring and in autumn. The negative peaks were related to the characteristic variations of SSTs with a sharp peak and a flat trough, which in turn deformed the sinusoidal SST variation of the annual cycle to enhance the asymmetry of the SST. The flat trough and the sharp peaks were most likely induced by the vertical structure of the water column. In winter, the temporal rate of surface temperature cooling decreases very weakly due to a quasi-homogeneous water column. By contrast, SST warming in summer can occur more rapidly than that in winter due to the shallower thermocline in summer. In light of this, stratification and/or bathymetry are other elements that may control the temperature variations at the sea surface (Xie et al. 2002).

In contrast to the pattern of the northern regions, the SSTAs of the Korea Strait, averaged over an area of about 50 km× 50 km (34.725–35.225° N, 129.725–130.225° E), were quite different from those in the northern area (Figure 5(*b*)). The SSTA scarcely showed semi-

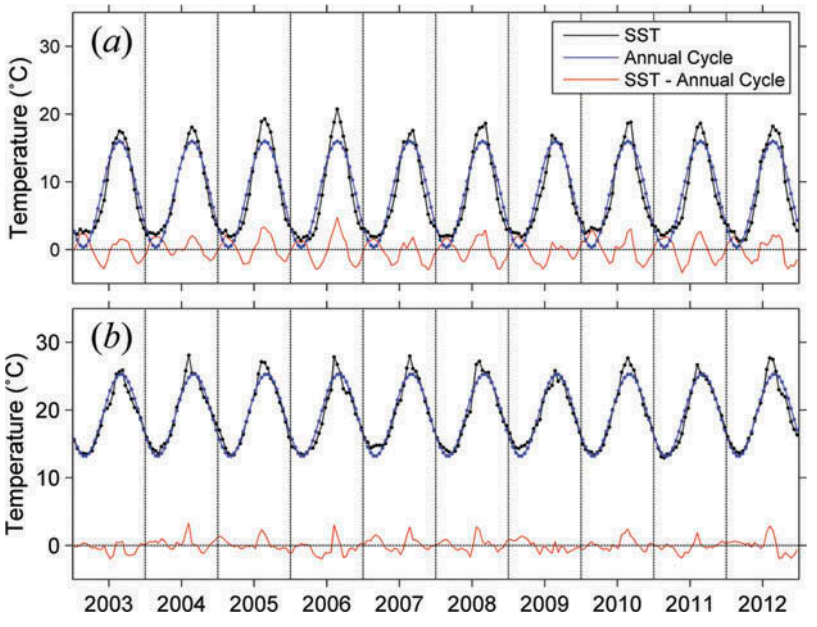

Figure 5. Time series of SST (black), annual cycle (blue), and differences between the two (SST minus annual cycle) (red) at (*a*) 47.2° N, 140.1° E near the Tatarskiy Strait and (*b*) 35° N, 130° E in the Korea Strait in the East/Japan Sea.

annual or other periodic oscillations. This implies that SST cooling contributing to the semi-annual cycle took place north of the SPF more favourably than it did south of the SPF.

Figure 6 shows the spatial distribution of the monthly SSTAs in spring and autumn. The negative SSTAs are dominant in May and November. In May, relatively large SSTAs of about −2°C occupied the Tatarskiy Strait and then abruptly decreased to between −1.5°C and −1.0°C in June. It should be noted that the core of these SSTAs with a local minimum migrated to a region farther south off the Primorye coast around 45° N. These SSTAs were likely induced by cold water mass-advected from the Tatarskiy Strait to the southwest. That is, the advection of the LCC from the Tatarskiy Strait to Vladivostok along the Russian coast (Martin and Kawase 1998) affected the SST cooling with spatial distinction over the continental shelf. In the southern region from the SPF, there were no peculiar structures, with small SST anomalies of about −0.5°C to 0.0°C noted in June (Figure 6).

The SSTAs in November revealed a distinct feature compared with those in spring. Negative anomalies (<−2°C) were distributed in the Tatarskiy Strait and on the Primorye coast as well as near Vladivostok (Figure 6(*c*)). Spring cooling was localized at the Tatarskiy Strait and partly off the Russian coast, whereas autumn cooling occurred in a much wider area north of the SPF. The cooling pattern in November is quite similar to the spatial distribution of the amplitudes of the semi-annual cycle. This implies that autumn cooling contributed to the semi-annual cycle more considerably than spring cooling. The cooling in autumn was not likely to be directly connected to the negative SSTAs in December. Thus, autumn cooling appears to be associated with direct wind forcing rather than remotely forced cooling, as in the pattern in spring. The cooling in November was greater than that in May by 20–30% in the region off the Russian coast and by 40–80% southwest of Vladivostok.

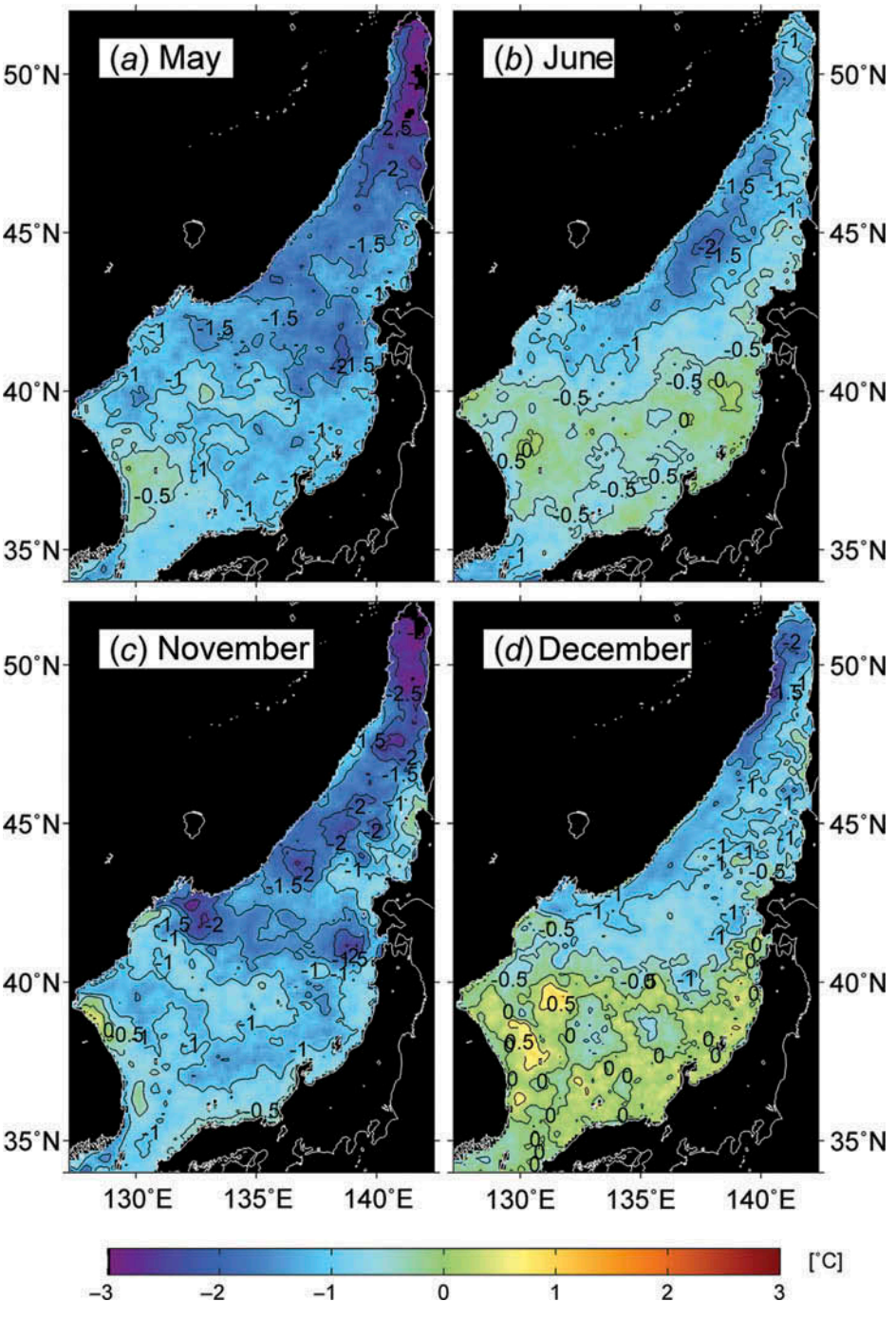

Figure 6. Distribution of SST residuals (°C) (SST minus annual cycle) at each grid in (*a*) May, (*b*) June, (*c*) November, and (*d*) December.

The SSTA south of the SPF in December shows positive values (Figure 6(*d*)). However, it implies not the warming of SST but the deviation of SST from an annual harmonic curve. The maximum positive SSTAs were detected in the entire area due to the flatness of the SST curve during winter and its sharpness in August. One of the potential candidates to explain the positive SSTA in December (Figure 6(*d*)) is the advection effect of the warm current system south of the SPF as shown in Figure 1. The transport of the warm current through the Korea Strait reaches a maximum not in summer but in October and a minimum in February (Takikawa, Yoon, and Cho 2005; Na et al. 2009; Ostrovskii et al. 2009; Fukudome et al. 2010). Many of the satellite drifters have shown its meandering south of the SPF from the Korea Strait to the Tsugaru Strait over a few months (Lee and Niiler 2005). Thus, the advection of the TWC can result in the distinction of SSTA between the southern and the northern regions in December (Figure 6(*d*)).

Our previous study has reported the spatial phase lag of about 24 days in SST cooling between the southern and the northern regions (Park et al. 2005). The phase lag of SST variations between north and south of the SPF can also generate positive SSTA in the southern region in December. The other candidate can be the effect of spatial distinction of MLD between north and south from the SPF, which is explained in the following section.

3.5. *Effect of wind on SST cooling*

3.5.1. *Distribution of wind speed*

First, we examined the role of wind field on SSTA variations or SST cooling in late autumn based on our hypothesis of the cooling process. Northwesterly wind begins to blow through the Vladivostok orographic gap in November and becomes the strongest during cold-air outbreak events in January (Dorman et al. 2004; Park et al. 2005). However, the maximum rate of SST cooling in the northern part of the EJS was not found in January or February with a dominant cold air outbreak but in November, i.e. at the beginning of winter (Park et al. 2005). Figure 7 shows the monthly climatology of the wind speeds of QuikSCAT from July 1999 to November 2008. In November, strong wind speeds greater than 9 m s^{-1} prevailed over the regions south of Vladivostok, west of the Tsugaru Strait, and west of Hokkaido. These regions, except for the area west of Hokkaido, coincided with areas with high semi-annual amplitudes, as shown in Figure 3.

Cooling of SST can occur from the coastal upwelling in the EJS, but it has been well known to take place at the limited coastal regions of the southeastern coast of Korea only in summer, A (Ulgi or Gampo) and B (Donghae) as marked in Figure 7(*a*) (Lee and Na 1985; Park and Kim 2010). The wind directions except for summer do not provide favourable conditions for coastal upwelling as shown in the wind distributions in May and November of Figure 7. Thus, SST cooling in November is not related to the coastal upwelling at the specific areas.

3.5.2. *Latent heat flux*

A wind field changes the SST through the processes of air–sea heat and momentum exchange, entrainment, upwelling, horizontal Ekman transport, Ekman pumping, and others. Under extreme events such as hurricanes or tropical storms, entrainment by turbulent mixing is the primary mechanism that lowers the SST, with the air–sea heat exchange playing only a minor role (Price 1981). However, in a general wind environment, Junge and Haine (2001) emphasized that the most effective way to alter the SST

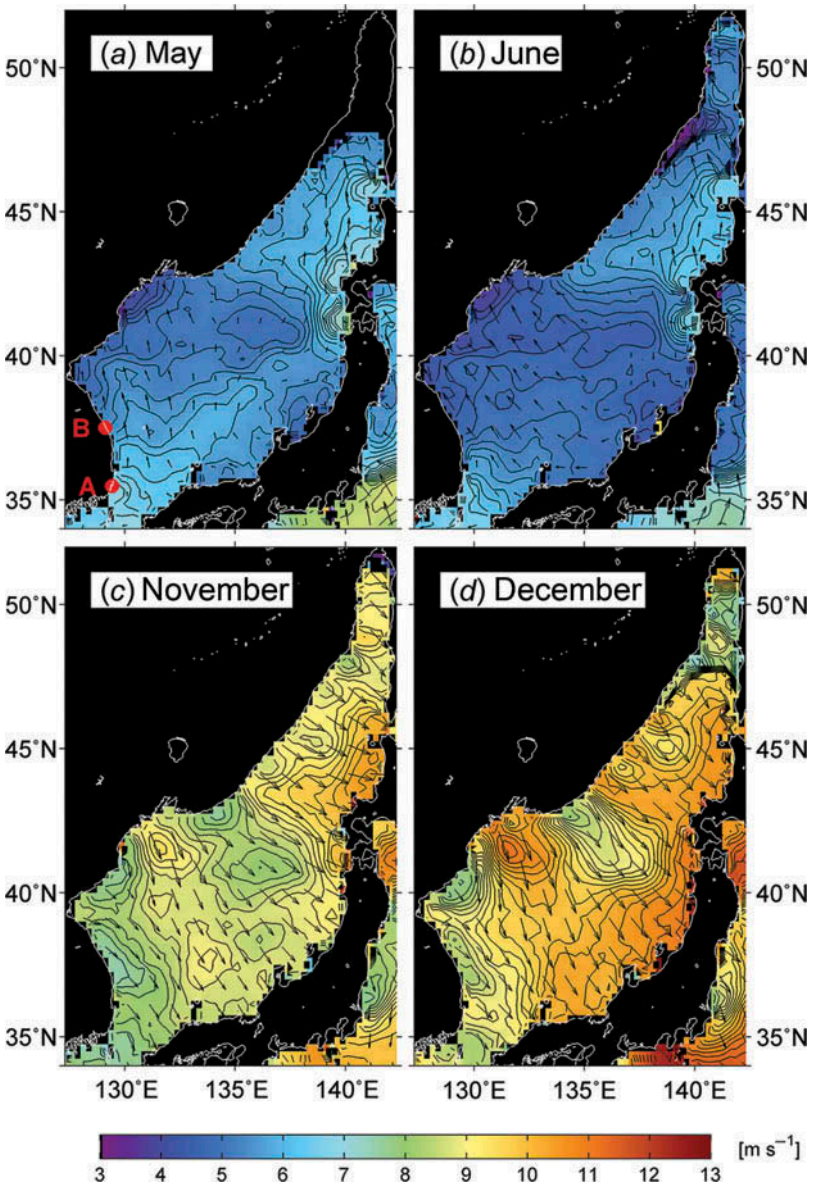

Figure 7. Monthly distribution of wind speed (m s^{-1}) climatology from QuikSCAT in (*a*) May, (*b*) June, (*c*) November, and (*d*) December for a decade from 1999 to 2008. The positions A (Ulgi or Gampo) and B (Donghae) denote the upwelling sites at the coastal area of Korea in summer.

was to change the local, simultaneous air–sea heat flux and wind stress, whereas other perturbations were ineffective in the North Atlantic.

The major constituents contributing to latent heat flux and sensible heat flux are the wind speed, specific humidity, and air–sea temperature difference. Because the latent heat flux was commonly larger than the sensible heat flux, we examined the monthly variation of NCEP/NCAR latent heat flux near the high-amplitude core (47° N, 140° E) off the Russian coast for a recent decade from 2003 to 2012 (Figure 8(*a*)). The 10 year averaged

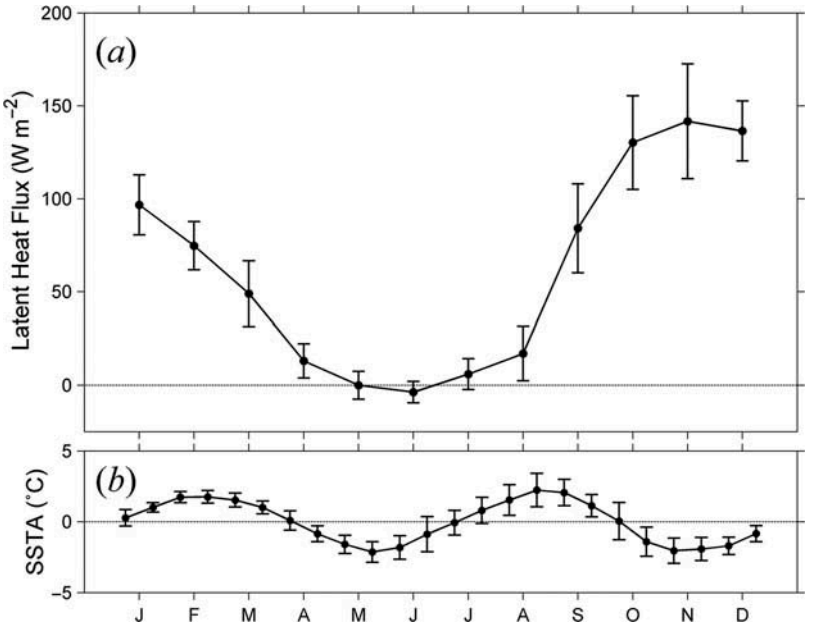

Figure 8. (*a*) Monthly variation of the latent heat flux (W m^{-2}) from NCEP data at a position (140° E, 47° N) off the Russian coast in the northeastern part of EJS from 2003 to 2012 and (*b*) the monthly variation of SST anomalies (°C), subtracting annual cycle from SSTs, where each error bar indicates standard deviation within each bin of time.

monthly variations of the latent heat flux at the sea surface, as denoted in Figure 8(*a*), showed obvious seasonality with a minimum in January and a maximum (~140 W m^{-2}) in November. Year-to-year variations of the latent heat flux (not shown here) exhibited a maximum in November or December during winter. The monthly mean of the SSTAs reached its lowest value of about −2.5°C in late November (Figure 8(*b*)), which was coincident with the time of the maximum latent heat flux. The coincidence of times between the maximum cooling and the maximum latent heat loss in the northern region implies that wind field played an important role in SST cooling in the northern regions with relatively large amplitudes of the semi-annual cycle.

Therefore, wind forcing seemed to be the most dominant factor controlling SST cooling at the beginning of winter or late autumn. This process would produce SST damping to generate a semi-annual SST cycle in an SST time series. If wind speed is one of the most important factors on changes in SST, we should determine a clear relation between year-to-year variations of SSTA and wind speed. We attempted to verify this from wavelet analysis in the following section.

3.5.3. Relation between wavelet spectra of SSTA and wind speed

To understand the year-to-year variations of SST, we applied wavelet analysis to both SST and SSTA as shown in Figures 9(*a*) and (*b*). Spectral energy of SST revealed dominant peaks at a period of 1 year (1 cycle per year (CPY)) whereas that of SSTA indicated a high spectral peak at a semi-annual frequency (0.5 year or 2 CPY). It is noted that the spectral powers of the semi-annual cycle of SSTA demonstrated obvious

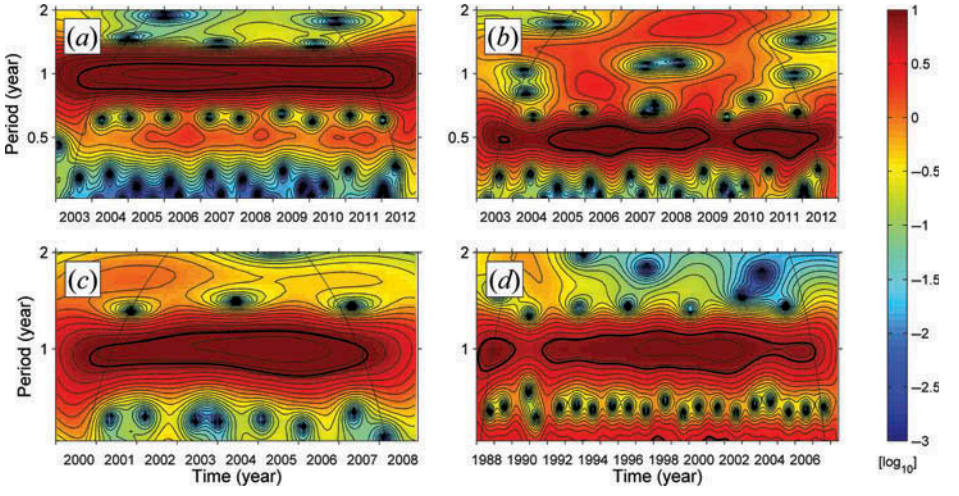

Figure 9. Wavelet spectrum of (*a*) MURSST, (*b*) SSTA from MURSST (2003–2012), (*c*) wind speed from QuikSCAT (2000–2008), and (*d*) sea-ice concentrations from SSM/I (1988–2008), where the thick solid line denotes 95% confidence level and the dashed curve indicates the cone of influence region of the wavelet spectrum.

year-to-year variations (Figure 9(*b*)), which has long been impossible from Fourier analysis. The wind field over the EJS also demonstrated dominant wavelet spectral powers at a period of 1 year (Figure 9(*c*)). If wind forcing plays an important role in SST cooling in autumn, we should obtain some coherence between the year-to-year variations of wind speeds in November and those of SSTAs from October to November in the EJS.

To testify this hypothesis, we investigated the wavelet spectral powers of SSTA and wind speed for the northern region of the EJS (>40° N, <140° E, except for the Tatarskiy Strait) corresponding to October and November from 2003 to 2008 during an overlapped period between MURSST (2003–2013) and QuikSCAT period (2000–2008). The wavelet spectral power demonstrated an obvious linear relationship between SSTA and wind speeds with a linearly regressed trend of about −2.05 (R^2 = 0.91) and with a correlation coefficient of about −0.95 (R^2 = 0.90) (Figure 10(*a*)). This implies that wind speed controls the cooling rates of SST in autumn. In addition, yearly averaged wavelet powers of SSTA difference between October and November (November minus October) from 2003 to 2008 also revealed negative dependence on those of wind speeds in November (Figure 10(*b*)).

Therefore, our analyses of wind field demonstrated that autumn cooling in the northern part of the EJS primarily resulted from direct and local wind forcing through the air–sea heat exchange. This supports our hypothesis on the significant role of wind speed in the cooling process in the EJS in late autumn.

3.6. Effect of MLD on autumn cooling

3.6.1. SST cooling to MLD difference

Surface cooling depends not only on the magnitude of the wind and heat loss but also on other oceanic conditions. One of the important oceanic factors is MLD. When MLD is

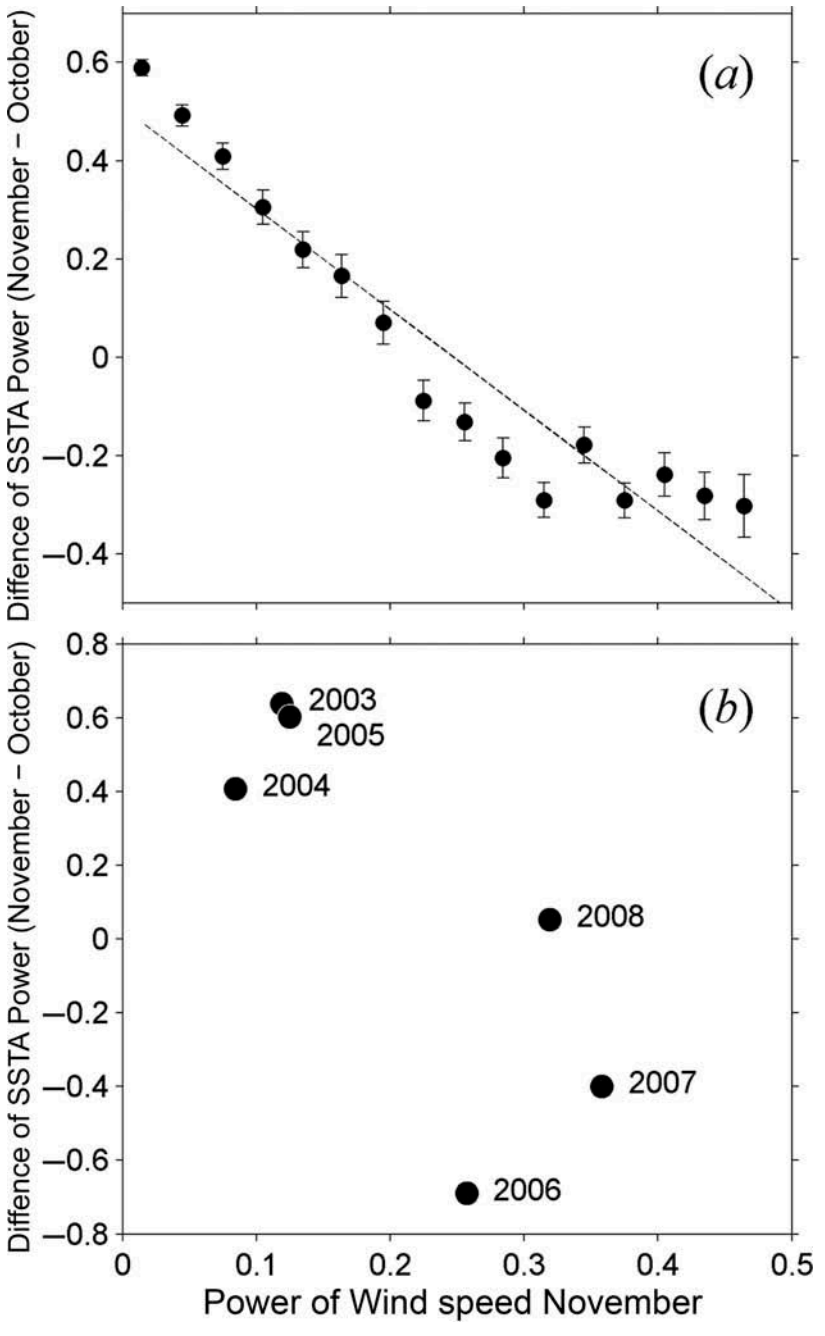

Figure 10. (*a*) Difference of wavelet spectral power of SSTA, November minus October, as a function of wavelet spectral power of wind speed at an area north of the SPF (>40° N, <140° E) in November, where the error bars correspond to standard deviation within a bin for average, and (*b*) the relationship of year-to-year variations of spectral powers of SSTA and wind speed at the same area of (*a*) from 2003 to 2008.

quite shallow, the oceanic response to atmospheric wind forcing will be relatively rapid, giving rise to a significant decrease of SST. Thermal inertia pertains to the temperature response of the water in the mixed layer subjected to time-varying heat or momentum flux at the sea surface (Yan, Shubel, and Pritchard 1990). Usually, a water mass with a high degree of thermal inertia shows a small change in its temperature. Thus, we hypothesized that regions with considerably high winds and small semi-annual amplitudes should be associated with a difference in the MLD distribution.

To investigate whether wind forcings and MLD affect SST cooling, we attempted to verify the hypothesis with relative MLD distribution to wind forcing using the following formulation of SST cooling:

$$\delta SST = \Delta Q / \rho_W C_P D. \tag{6}$$

Here, δSST is the temporal difference in the SST between two subsequent months, ΔQ is the net heat flux, ρ_W is the water density, C_P is the specific heat, and D is the MLD (Luis and Kawamura 2002).

The importance of MLD on cooling of water temperature can be understood from changes in the vertical temperature profile in Figure 11. Figures 11(*a*) and (*b*) show the vertical profiles of temperatures in the upper 200 m layer at two arbitrary locations near Vladivostok (T_N: 42.125° N, 131.125° E) in the northern area and at the Ulleung Basin (T_S: 35.875° N, 130.875° E) in the southern area from October to March next year. The differences between the cooling rates of the northern ($\delta T_N = T_N\,(Oct) - T_N\,(Nov)$) and southern ($\delta T_S = T_S\,(Oct) - T_S\,(Nov)$) areas, $\delta T_N - \delta T_S$, amounted to the highest value of about 3.32°C (Figure 11(*c*)). Such a difference of cooling rates lasted until December; however, it reversed to negative values after January. This implies that SSTs in the northern region tended to decrease much more rapidly than those in the southern region at an initial stage of cooling process, but less after January in which the MLD became sufficiently deep.

Both temporal variations of δSST_N (6.2°C per a month) and δSST_S from the WOA database also demonstrated the highest significant coolings (2.9°C per a month) at the sea surface from October to November (Figures 11(*d*) and (*e*)). MURSST showed a similar tendency as verified from the red lines in Figures 11(*d*)–(*f*). Difference of cooling rates between the northern and southern regions, $\delta SST_N - \delta SST_S$ (Figure 11(*f*)), changed to a negative value, which corresponded to slower cooling in the northern region than that in the southern region in winter. What generates the slow cooling in the northern region in winter? This might be associated with MLD. Figure 11(*g*) reveals the relationship between monthly variations of δSST_N (blue) and δSST_S (red) as a function of MLD. The highest rate of surface cooling was detected from October to November. As MLD became deep, the magnitude of temperature cooling rate at the sea surface tended to be decreased. In light of this, the MLD is anticipated to contribute to partly control the cooling rate of seawater at the sea surface.

3.6.2. *Spatial ratio of pseudo-MLD from wind and SST cooling*

Substantially, the heat flux linearly depends on the wind speed. Under this assumption and conditions of a constant water density and specific heat capacity in Equation (6), it is possible to obtain pseudo-MLD indirectly using the SST difference and wind speed W, as follows:

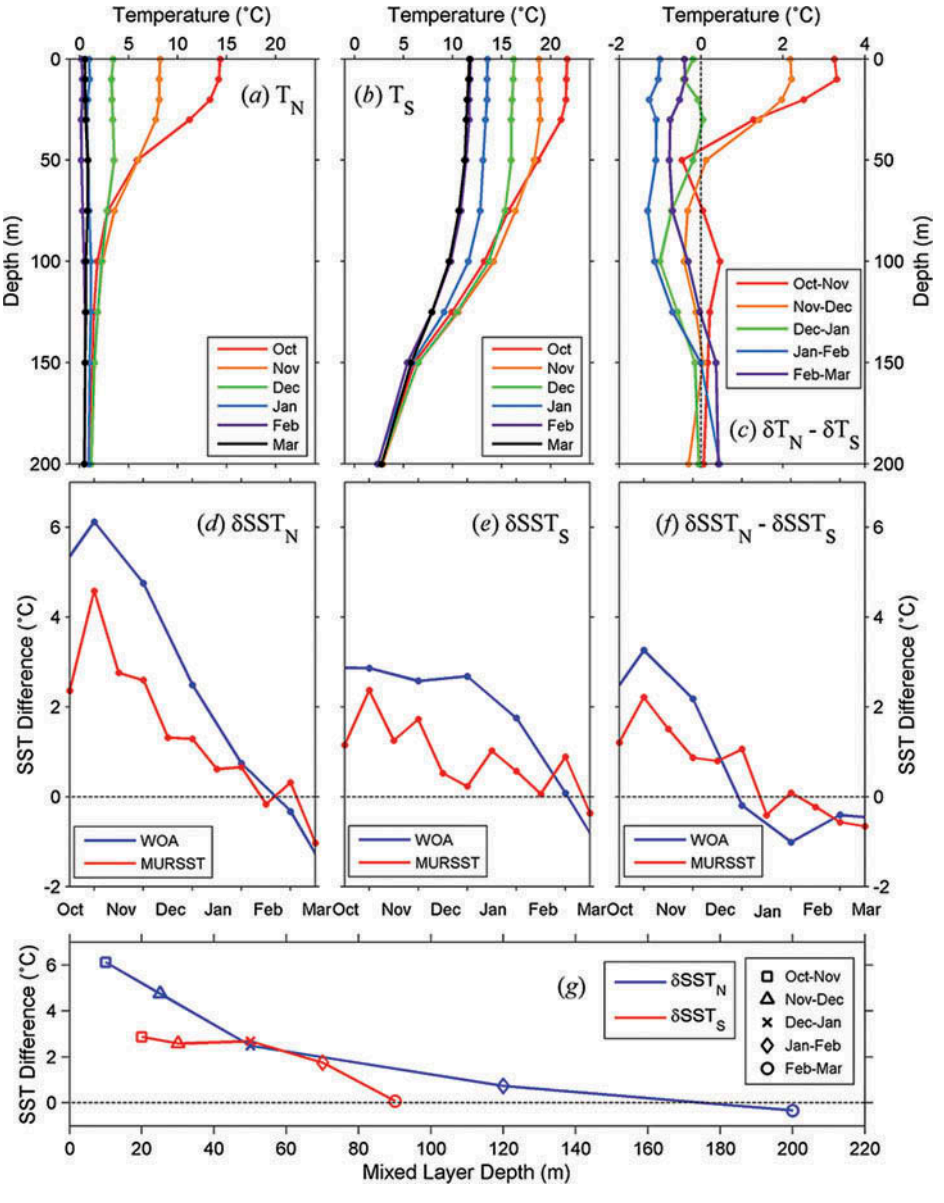

Figure 11. Monthly variations of vertical water-temperature (°C) profile at an arbitrary location (*a*) near Vladivostok (42.125° N, 131.125° E) and (*b*) in the TWC region (35.875° N, 130.875° E) from October to March next year, and (*c*) monthly distributions of the differences of SST cooling rates (present month – previous month) between the northern and the southern areas. Comparisons of time series of SST cooling rates at (*d*) the northern and (*e*) the southern areas between two adjacent months from October to March, (*f*) the differences of the SST cooling rates between the northern and the southern regions, where the SST data denoted by the blue (red) line were obtained from WOA (MURSST), respectively, and (*g*) monthly variations of SST difference at the northern (blue) and southern (red) areas as a function of MLD.

$$D_{pseudo} \sim \Delta Q/(\rho_W C_P \delta SST) \propto W/\delta SST. \quad (7)$$

The ratio shown in Equation (7) is not coincident with the exact MLD, so herein we called it the pseudo-MLD (D_{pseudo}). If the SST cooling depends on MLD, we should obtain the spatial pattern of pseudo-MLDs similar to the MLD distribution in the entire area of the East Sea from the modified Equation (7). According to our scale analysis of each parameter in Equation (7), the water density, ρ_W, did not substantially modify the spatial distribution of the ratios. So, we neglected the water density in Equation (7). D_{pseudo} can be easily obtained only with satellite data such as wind speed and SST data. Such a ratio is expected to explain the relative distribution of the MLD in the EJS in an indirect way.

Figure 12(a) shows the ratios of the QuikSCAT wind speed W to the temporal temperature change δSST between October and November. Herein, the unit is meaningless and only the relative magnitude is important to compare the relative MLDs. A small ratio implies that wind forcing has more of an effect on SST cooling in autumn. In the region southeast of Vladivostok, this ratio was small, approximately 2. By contrast, the warm side south of the SPF showed relatively large ratios in the range of 3–8. Large ratios appeared along the Japanese coast by a factor of 5 or more, which were at least twice as deep as the MLDs over the Japan Basin (Figure 12(*a*)).

This trend is in good agreement with a previous report on the MLD and thermocline depth between the south and north of the SPF (Chu, Lan, and Fan 2001). The distribution of the MLD from the WOA database in Figure 12(*b*) shows the spatial contrast between the

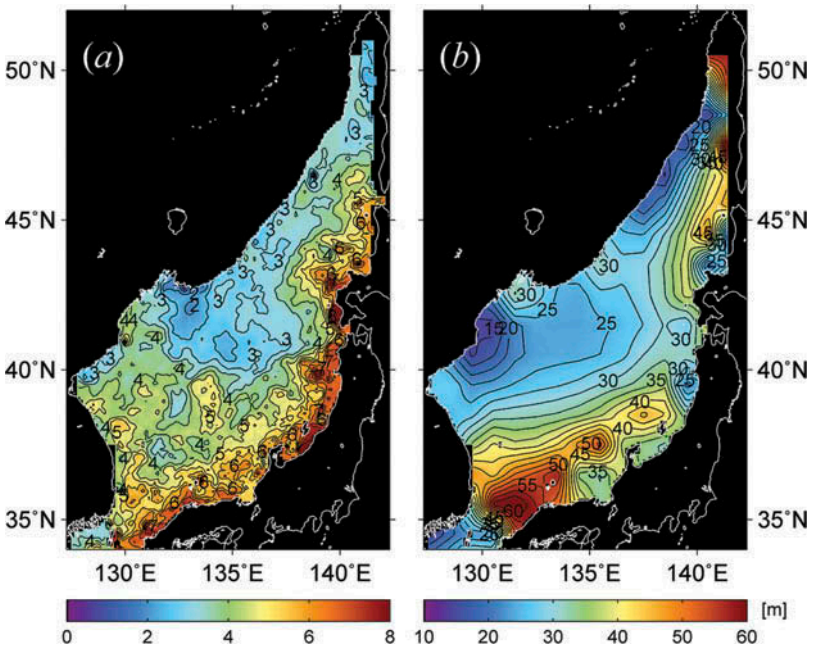

Figure 12. Spatial distribution of (*a*) the ratio (pseudo-MLD) in Equation (7), wind speed (m s^{-1}) to temporal SST difference (°C) in November and (*b*) MLD (m) from WOA in the East/Japan Sea.

continental side along the Russian and Korean coasts and the eastern side along the Japanese coast. The spatial distinction shown here is quite similar to the relative ratios in Figure 12(*a*).

The MLDs were relatively deep in the regions south of the SPF compared to the regions north of the SPF. Owing to the depth of the MLD and the continual supply of the TWC from the Korea Strait, the SST cooling in the southern area appears to be weak in late autumn. Such weak cooling will ultimately result in a small variance of the semi-annual cycle, as shown in Figure 2(*a*). Similarly, despite the prominent winds of about 10 m s^{-1} (Figure 7), the small SST amplitudes of the semi-annual cycle west of Hokkaido were likely caused by the relatively deep MLD and by the northward-flowing TWC approximately 138° E west of the Soya Strait (Figure 12(*a*)). The estimated pseudo-ratios of MLD were five or six times as deep as those southeast of Vladivostok at an earlier stage of cooling in November. The large ratios may be related to an increase in the thermal inertia from the deep MLD that produced only a small SST response at the sea surface. Therefore, the cooling rate at the sea surface is believed to be closely associated with MLD under the condition of similar atmospheric forcing. Thus, our analysis confirmed that the MLD played a partially important role in the SST responses at the sea surface.

3.7. *Effect of sea-ice melting on spring cooling*

3.7.1. *Southwestward-flowing cold current along the Russian coast*

As a main cause of semi-annual cycle in the northern part of the EJS, we showed earlier that the air–sea heat transfer by wind forcing was mostly responsible for autumn cooling at the sea surface. However, the wind field in May and June is relatively weak at about 5 m s^{-1} north of the SPF, accounting for approximately 30–50% of the wind speed in November (Figure 7). It is too small to account for the cooling process related to the high semi-annual amplitudes in Figure 3(*a*). Our hypothesis is that the spring cooling in the northern part of the EJS, especially along the Russian coast, took place due to the advected cold waters of the southwestward-flowing LCC as generated by the melting of sea ice in the Tatarskiy Strait.

Figure 13(*a*) exhibits the mean surface current vectors from satellite-tracked surface drifter data of Atlantic Oceanographic and Meteorological Laboratories (AOML). The current vectors revealed a cyclonic gyre over the Japan Basin as coincident with the previous studies (e.g. Yoon 1982). It should be also noted that such current vectors off the Russian coast tended to proceed to the southwest along the Russian coast at which the magnitude of the maximum mean current amounted to 0.2 m s^{-1}. This coincides with the results of Martin and Kawase (1998) addressing that ice edge melting in the Tatarskiy Strait generated an oceanic frontal structure and a westward geostrophic current, which fed into the LCC flowing from northeast to southwest along the Russian coast.

3.7.2. *Progress of low-salinity water along the Russian coast*

To confirm the southwestward current of sea-ice melted waters, we plotted monthly variations of surface salinity along the Russian coast from WOA climatology data, marked in red dots in Figure 13(*a*). The along-coast surface salinity revealed high freshening from March to May from 44° N to 48° N (Figure 13(*b*)). The salinity values at 48° N progressively reduced from March (34.1 psu) to April (33.7 psu), and reached the

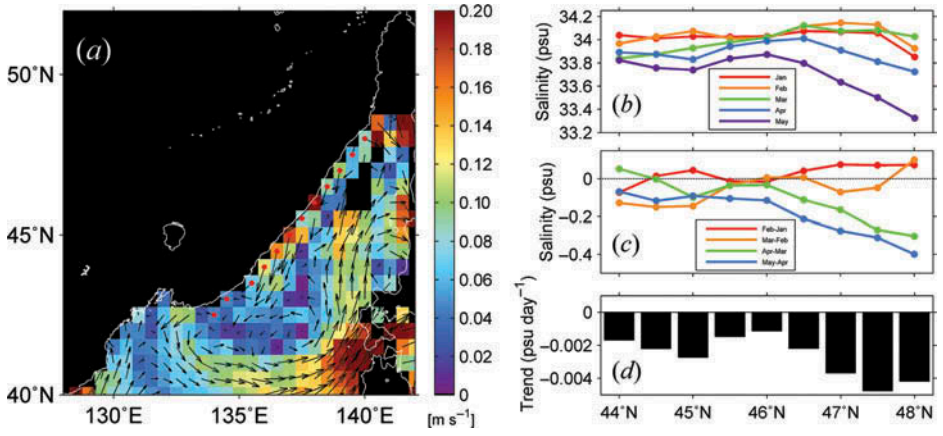

Figure 13. (*a*) Distribution of surface currents (m s^{-1}) from AOML climatology, (*b*) salinity profiles at positions along the Russian coast as designated in red dots from January to May, (*c*) their differences between the two adjacent months (latter minus former), and (*d*) a trend of salinity variations (psu day^{-1}) as a function of latitude from 44° N and 48° N at the coastal area.

lowest peak in May (33.3 psu) (Figure 13(*b*)), which was clear evidence of the appearance of sea-ice melted water off the Russian coast. The salinity difference at 48° N amounted to −0.4 psu between April and May (Figure 13(*c*)). All of the salinity values along the Russian coast from 44° N to 48° N showed a negative trend (−0.005 to −0.001 psu day^{-1}) from January to May (Figure 13(*d*)). This confirms that the fresh and cold waters from sea-ice melting at the Tatarskiy Strait advected to the southwest and continuously flowed along the Russian coast in spring.

Martin and Kawase (1998) suggested that the freshwater flux associated with the southward ice transport in the Tatarskiy Strait might contribute to the driving of the LCC. Owing to the freshening of sea-ice melted cold water along the Russian coast in spring, there was a temporal phase lag of 1–2 months between sea-ice melting in April and the appearance of negative semi-annual SST anomalies along the continental shelf in May (Figure 6(*a*)) and June (Figure 6(*b*)). In addition, such a southwestward flow generates spring bloom as evidenced from the analysis of satellite-observed chlorophyll-*a* concentration data (Park, Chae, and Park 2013). Thus, all of these correspondences confirmed to us that semi-annual amplitudes of SST variations along the continental shelf off Russia in spring were induced by non-local, remotely forced sea-ice melted cold water.

3.8. *Asymmetry of SST variations*

3.8.1. *Kurtosis*

We have shown that the semi-annual cycle in the northern EJS was mainly caused by deviations from the symmetric sinusoidal curves. We quantified the characteristics of asymmetry with the statistical parameters of kurtosis and skewness. The skewness is referred to the third moment of the distribution and the degree of asymmetry of the data about the mean and the kurtosis is a non-dimensional number measuring the flatness or peakedness of a distribution (Emery and Thomson 1998).

Figure 14(*a*) shows the kurtosis of the temporal variations of SSTs on each grid. The kurtosis ranged from 1.5 to 2.5 over the basin. High kurtosis with values greater than 2

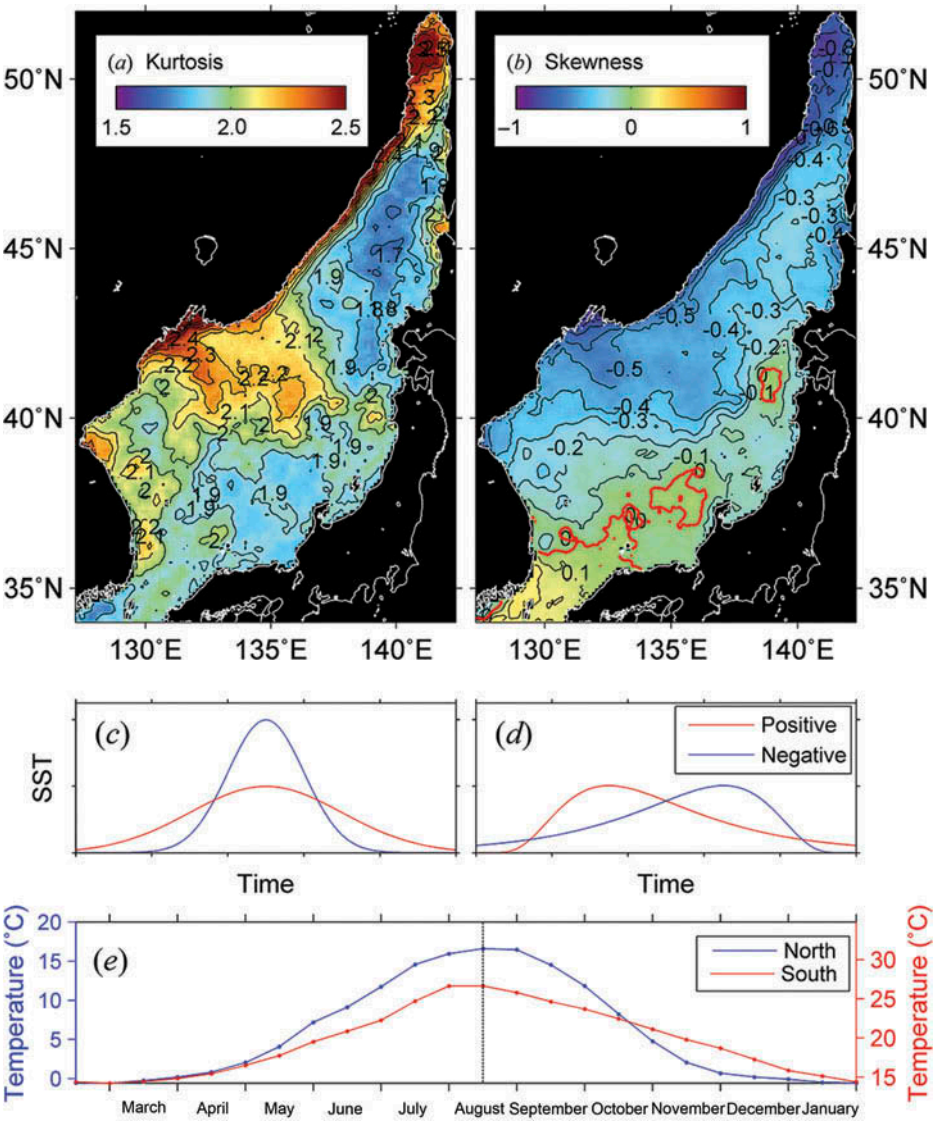

Figure 14. Spatial distribution of (*a*) kurtosis and (*b*) skewness of SST variations, where the red line represents skewness lines with zero value, the conceptual curves of SST (°C) (*c*) with high (blue) and low (red) kurtosis and (*d*) with negative (blue) and positive (red) skewness, and (*e*) monthly averaged SST (°C) variations near the Tatarskiy Strait (blue) and the Korea Strait (red).

appeared in the Tatarskiy Strait, along the Primorye coast over the continental shelf, south of Vladivostok, over the Japan Basin, along the eastern coast of Korea, and the East Korea Bay off North Korea (Figure 14(*a*)). That is, the SST curves of these regions have a sharp shape corresponding to high kurtosis as shown by the blue curve in Figure 14(*c*). In contrast, low values of kurtosis (<2) were detected in the regions west of Hokkaido and south of the SPF. This implies that SSTs in the southern region of the EJS have a relatively flat peak as illustrated by the red curve with low kurtosis in Figure 14(*c*). As both spring cooling and autumn cooling increased, the kurtosis tended to increase. The

spatial pattern with relatively high kurtosis (>2) demonstrated good agreement with that of the semi-annual cycle with high amplitudes (>2°C) north of the SPF.

3.8.2. *Skewness*

In addition to the kurtosis, the skewness of SST variations can be also used as a measure of asymmetric characteristics of temporal variation of SST. In some cases, the SST variations that contained the same kurtosis may be skewed to the left or right. The skewness can determine the direction of the obliqueness of the seasonal SST curve. Figure 14(*b*) represents the spatial distribution of the skewness value on each grid. Most of the skewness values in the basin were negative except for the regions near the Korea Strait and in the southern portion of the EJS. SST variations with negative skewness are represented by the blue line in Figure 14(*d*). The seasonal SST curve in Figure 5(*b*) shows asymmetry with a rapid increase in the SST. Its peak came earlier than the peak of the annual cycle. This shape was similar to that created by the red line in Figure 14(*d*), which coincided with the positive skewness in the southern region of the EJS.

The monthly variations of the SSTs presented the distinction between the northern and the southern regions of the EJS in terms of kurtosis and skewness (Figure 14(*e*)). Figures 14(*c*) and (*d*) were exaggerated as a typical example of conceptual distribution of skewness and kurtosis. When one keeps an eye on the rapid increasing of SST (the red line) prior to the maximum SST (the dash line) in mid-August and then the slow decreasing of SST (Figure 14(*e*)), one can find its similarity to the red line (positive skewness) in Figure 14(*d*). Therefore, we may conclude that the shapes of the temporal variations of SSTs are seasonally asymmetric depending on the cooling process exerted on each location in the EJS.

3.8.3. *Ratio of semi-annual cycle to annual cycle*

We suggest herein that the ratio between the semi-annual and annual cycle should be used as a means of understanding how much the SST variations are asymmetric and how much they deviate from the annual cycle. The ratio R_{12} is given as

$$R_{12} = \frac{C_2}{C_1}, \tag{8}$$

where C_1 and C_2 are the amplitudes of the annual and semi-annual cycles of the SST variations, respectively. We presented the ratio as a percentage in Figures 2(*b*) and (*d*). In general, the ratios are not greater than 1 at mid-latitude regions. As the ratio approaches zero, the SST variation approaches a simple sinusoidal curve. By contrast, as it increases, the asymmetry will tend to increase with a short and sharp peak in summer and a long and flat winter period. Thus, it is expected that we can understand the degree of SST asymmetry by discerning the relative strength of the semi-annual cycle to the annual cycle.

4. Summary and conclusion

In a majority of oceans, the seasonal variations of SSTs consist mainly of the annual and semi-annual variations. Because an SST change is a consequence of diverse forcings such

as air–sea heat flux exchanges, oceanic currents, mixing processes, oceanic circulation, solar insolation, and others, changes in forcings will tend to generate changes in seasonal and year-to-year variations of SSTs by modifying the annual curve of the SST variations each year. Then, such changes will create the semi-annual cycle of the SST as an immediate footprint on SST time series, ultimately leading to asymmetry in the seasonal SST curve. Accordingly, an investigation of the semi-annual SST cycle may be a good tool with which to understand not only SST cooling but also primary atmospheric wind forcing. To test this hypothesis on the seasonal changes of the SST and examine their possible causes, we derived the harmonics of satellite-based SST variations to survey the characteristics of the semi-annual cycle and the asymmetry of the SST curve with respect to time.

This study presented the spatial structures of the amplitudes, phases, and variances of the semi-annual SST cycle in the EJS, which has thus far remained unexplored. Relatively high amplitudes of 1.6–3.0°C were noted in the north of the SPF, whereas the result was not significant in the regions south of the SPF, with small amplitudes of 0.2–1.4°C. In particular, the amplitudes were significant in the Tatarskiy Strait and along the continental shelf off the Russian coast, where the total variance of the SST was 8% and reached 25% as regards the amplitudes of the annual frequency. Areas with relatively high semi-annual cycles were correlated to places with strong wind fields as a major contributor to the air–sea heat flux in late autumn. The MLD difference played an important role in the SST responses at the beginning of the cooling process, as verified by the ratio between the wind speed and the temporal SST change, i.e. the effect of the wind field on oceanic temperature response.

It was also noted that the semi-annual cycle in the EJS was produced not by a real semi-annual forcing but by two different annual forcings that appeared at different times with a 6 month interval per year. That is, the frequency of forcings was not semi-annual but rather substantially annual. Processes related to SST cooling recurring semi-annually were quite different in the northern part of the EJS. We showed that cooling in autumn was locally caused by atmospheric wind forcings during the onset of cold northwesterly wind, while cooling in spring was remotely caused by cold water advection over the continental shelf from sea-ice melting in the Tatarskiy Strait as noted in earlier studies.

We presented the characteristic parameters of the SST asymmetry with kurtosis and skewness, which has never been documented in the EJS. High kurtosis with values greater than 2 were found north of the SPF, such as those near the Tatarskiy Strait, along the Primorye coast, and south of Vladivostok, in contrast to the southern regions showing low kurtosis. The skewness values were mostly negative, which indicated that the SST distribution skewed to the right with a short tail after the seasonal peak of the SST variation. If a warm current system such as the EKWC along the eastern coast of Korea and the TWC develops significantly, SSTs will experience abnormal warming given the positive skewness values shown for the Korea Strait and the southern part of the East Sea. On the other hand, if the cooling process is predominant as compared to normal years, the skewness will be likely shifted to a negative value.

Since the semi-annual SST cycle substantially stemmed from the asymmetry of the sinusoidal SST variations with a smooth trough in winter with rapid cooling, we suggest that the ratio of the semi-annual amplitude to the annual amplitude of the SST harmonics can be used as a typical indicator of SST asymmetry. Thus, the semi-annual cycle is expected to enhance our understanding and knowledge of regional inconsistencies in the highly variable year-to-year SST variations in the EJS. This study did not deal with the

detailed process of SST warming with a sharp crest in summer, which will be further studied in the future.

Acknowledgements

The authors greatly appreciate unknown reviewers for their invaluable comments.

Funding

This study was supported by the National Meteorological Satellite Centre [Project no. 153-3100-3137-302-210-13]. Data processing was supported by the 'East Asian Seas Time series-I (EAST-I)' and the 'Long-term change of structure and function in marine ecosystems of Korea' projects funded by the Ministry of Oceans and Fisheries, Korea.

References

Chen, S. S., W. Zhao, J. E. Tenerelli, R. H. Evans, and V. Halliwell. 2001. "Impact of the AVHRR Sea Surface Temperature on Atmospheric Forcing in the Japan/East Sea." *Geophysical Research Letter* 28 (24): 4539–4542.

Chin, T. M., J. Vazquez, and E. Armstrong. 2013. "A Multi-Scale, High-Resolution Analysis of Global Sea Surface Temperature." In *Algorithm Theoretical Basis Document, Version 1.3*, 13 p. Pasadena, CA: Jet Propulsion Laboratory.

Chu, P. C., Y. C. Chen, and S. H. Lu. 1998. "Temporal and Spatial Variabilities of Japan Sea Surface Temperature and Atmospheric Forcings." *Journal of Oceanography* 54 (3): 273–284.

Chu, P. C., J. Lan, and C. Fan. 2001. "Japan Sea Thermohaline Structure and Circulation. Part I. Climatology." *Journal of Physical Oceanography* 31: 244–271.

Defant, A. 1961. *Physical Oceanography I*. New York: Pergamon Press.

Dorman, C. E., R. C. Beardsley, N. A. Dashko, C. A. Friehe, D. Khelif, K. Cho, R. Limeburner, and S. M. Varlamov. 2004. "Winter Marine Atmospheric Conditions over the Japan/East Sea." *Journal of Geophysical Research* 109: 1–26.

Elsayed, M. 2010. "An Overview of Wavelet Analysis and Its Application to Ocean Wind Waves." *Journal of Coastal Research* 26 (3): 353–540.

Emery, W. J., and R. E. Thomson. 1998. *Data Analysis Methods in Physical Oceanography.* Amsterdam: Pergamon Press.

Fukudome, K.-I., J.-H. Yoon, A. Ostrovskii, T. Takikawa, and I.-S. Han. 2010. "Seasonal Volume Transport Variation in the Tsushima Warm Current through the Tsushima Straits from 10 Years of ADCP Observations." *Journal of Oceanography* 66 (4): 539–551.

Ichiye, T. 1984. "Some Problems of Circulation and Hydrography of the Japan Sea and the Tsushima Current." *Ocean Hydrodynamics of the Japan and East China Seas* 39: 15–54.

Joanes, D. N., and C. A. Gill. 1998. "Comparing Measures of Sample Skewness and Kurtosis." *Royal Statistical Society* 47 (1): 183–189.

Junge, M. M., and T. W. N. Haine. 2001. "Mechanisms of North Atlantic Wintertime Sea Surface Temperature Anomalies." *Journal of Climate* 14: 4560–4572.

Kawabe, M. 1982. "Branching of the Tsushima Current in the Japan Sea, Part I. Data Analysis." *Journal of the Oceanographical Society of Japan* 38: 95–107.

Kawamura, H., and P. Wu. 1998. "Formation Mechanism of Japan Sea Proper Water in the Flux Center off Vladivostok." *Journal of Geophysical Research* 103 (C10): 21611–21622.

Kelly, K. A. 1988. "Comment on 'EOF Analysis of Advanced Very High Resolution Radiometer Surface Temperature Patterns in Santa Barbara Channel' by Gary S. E. Lagerloef and Robert L. Bernstein." *Journal of Geophysical Research* 93: 15753–15754.

Kim, K., K. R. Kim, D. H. Min, Y. Volkov, J. H. Yoon, and M. Takematsu. 2001. "Warming and Structural Changes in the East (Japan) Sea: A Clue to Future Changes in Global Oceans?" *Geophysical Research Letter* 28 (17): 3293–3296.

Lagerloef, G. S. E., and R. L. Bernstein. 1988. "Empirical Orthogonal Function Analysis of Advanced Very High Resolution Radiometer Surface Temperature Patterns in the Santa Barbara Channel." *Journal of Geophysical Research* 93: 6863–6873.

Lee, D.-K., and P. P. Niiler. 2005. "The Energetic Surface Circulation Patterns of the Japan-East Sea." *Deep-Sea Research II* 52 (11–13): 1547–1563.

Lee, J. C., and J. Y. Na. 1985. "Structure of Upwelling off the Southeast Coast of Korea." *The Journal of the Oceanological Society of Korea* 20 (3): 6–19.

Liu, P. C., and G. S. Miller. 1996. "Wavelet Transforms and Ocean Current Data Analysis." *Journal of Atmospheric and Oceanic Technology* 13 (5): 1090–1099.

Luis, A. J., and H. Kawamura. 2002. "The Study of Sea Surface Temperature – Cooling Dynamics near the Indian Tip during May 1997." *Journal of Geophysical Research* 107 (C10): 3171–3181.

Martin, S., and M. Kawase. 1998. "The Southern Flux of Sea Ice in the Tatarskiy Strait, Japan Sea and the Generation of the Liman Current." *Journal of Marine Research* 56: 141–155.

Martin, S., E. Munoz, and R. Drucker. 1992. "The Effect of Severe Storms on the Ice Cover of the Northern Tatarskiy Strait." *Journal of Geophysical Research* 97 (C11): 17753–17764.

Meyers, S. D., B. G. Kelly, and J. J. O'Brien. 1993. "An Introduction to Wavelet Analysis in Oceanography and Meteorology: with Application to the Dispersion of Yanai Waves." *Monthly Weather Review* 121 (10): 2858–2866.

Minobe, S., A. Sako, and M. Nakamura. 2004. "Interannual to Interdecadal Variability in the Japan Sea Based on A New Gridded Upper Water Temperature Data Set." *Journal of Physical Oceanography* 34: 2382–2397. doi:10.1175/JPO2627.1.

Monterey, G., and S. Levitus. 1997. "Seasonal Variability of Mixed Layer Depth for the World Ocean." In *NOAA Atlas NESDIS 14*, 96 p. Washington, DC: US Government Printing Office.

Na, H., Y. Isoda, K. Kim, Y. H. Kim, and S. J. Lyu. 2009. "Recent Observations in the Straits of the East/Japan Sea: A Review of Hydrography, Current and Volume Transports." *Journal of Marine Systems* 78 (2): 200–205.

Ostrovskii, A. G., K. Fukudome, J.-H. Yoon, and T. Takikawa. 2009. "Variability of the Volume Transport through the Korea/Tsushima Strait As Inferred from the Shipborne Acoustic Doppler Current Profiler Observations in 1997–2007." *Oceanology* 49 (3): 338–349.

Park, K.-A., H.-J. Chae, and J.-E. Park. 2013. "Characteristics of Satellite Chlorophyll-A Concentration Speckles and A Removal Method in A Composite Process in the East/Japan Sea." *International Journal of Remote Sensing* 34 (13): 4610–4635.

Park, K.-A., J. Y. Chung, and K. Kim. 2004. "Sea Surface Temperature Fronts in the East (Japan) Sea and Temporal Variations." *Geophysical Research Letter*, 31: L07304. doi:10.1029/2004gl019424.

Park, K.-A., J. Y. Chung, K. Kim, and B. H. Choi. 1994. "A Study on Comparison of Satellite Drifter Temperature with Satellite Derived Sea Surface Temperature of NOAA/NESDIS." *Journal of Korean Society of Remote Sensing* 11 (2): 83–107.

Park, K.-A., J. Y. Chung, K. Kim, B. H. Choi, and D. K. Lee. 1999. "Sea Surface Temperature Retrievals Optimized to the East Sea (Sea of Japan) Using NOAA/AVHRR Data." *Marine Technology Society Journal* 33 (1): 23–35.

Park, K.-A., J. Y. Chung, K. Kim, and P. C. Cornillon. 2005. "Wind and Bathymetric Forcing of the Annual Sea Surface Temperature Signal in the East (Japan) Sea." *Geophysical Research Letter* 32: L05610. doi:10.1029/2004gl022197.

Park, K.-A., K. Kim, P. C. Comillon, and J. Y. Chung. 2006. "Relationship between Satellite-Observed Cold Water along the Primorye Coast and Sea Ice in the East Sea (The Sea of Japan)." *Geophysical Research Letter* 33: L10602. doi:10.1029/2005GL025611.

Park, K.-A., and K.-R. Kim. 2010. "Unprecedented Coastal Upwelling in the East/Japan Sea and Linkage to Long-Term Large-Scale Variations." *Geophysical Research Letters* 37: L09603. doi:10.1029/2009GL042231.

Park, K.-A., K.-R. Kim, K. Kim, J. Y. Chung, and P. C. Cornillon. 2003. "Comparison of the Wind Speed from An Atmospheric Pressure Map (Na Wind) and Satellite Scatterometer-Observed Wind Speed (NSCAT) over the East (Japan) Sea." *Journal of the Korean Society of Oceanography* 38 (4): 173–184.

Park, K.-A., E.-Y. Lee, S.-R. Chung, and E.-H. Sohn. 2011. "Accuracy Assessment of Sea Surface Temperature from NOAA/AVHRR Data in the Seas around Korea and Error Characteristics." *Korean Journal of Remote Sensing* 27 (6): 663–675.

Park, K.-A., J.-E. Park, B.-J. Choi, D.-S. Byun, and E.-I. Lee. 2013. "An Oceanic Current Map in the East Sea for Science Textbooks Based on Scientific Knowledge Acquired from Oceanic Measurements." *Journal of the Korean Society of Oceanography* 18 (4): 234–265.

Park, K.-A., F. Sakaida, and H. Kawamura. 2008a. "Error Characteristics of Satellite-Observed Sea Surface Temperatures in the Northeast Asian Sea." *Journal of Korean Society of Earth Science* 29 (3): 280–289.

Park, K.-A., F. Sakaida, and H. Kawamura. 2008b. "Oceanic Skin-Bulk Temperature Difference through the Comparison of Satellite-Observed Sea Surface Temperature and In-Situ Measurements." *Korean Journal of Remote Sensing* 24 (4): 1–15.

Price, J. F. 1981. "Upper Ocean Response to A Hurricane." *Journal of Physical Oceanography* 11: 153–175.

Provost, C., O. Garcia, and V. Garcon. 1992. "Analysis of Satellite Sea Surface Temperature Time Series in the Brazil-Malvinas Current Confluence Region: Dominance of the Annual and Semiannual Periods." *Journal of Geophysical Research* 97 (C11): 17841–17858.

Qu, T., J. Gan, A. Ishida, Y. Kashino, and T. Tozuka. 2008. "Semiannual Variation in the Western Tropical Pacific Ocean." *Geophysical Research Letter* 35: L16602. doi:10.1029/2008gl035058.

Sakaida, F., and H. Kawamura. 1992a. "Estimation of Sea Surface Temperatures around Japan Using the Advanced Very High Resolution Radiometer (AVHRR)/NOAA-11." *Journal of Oceanography* 48: 179–192.

Sakaida, F., and H. Kawamura. 1992b. "Accuracies of NOAA/NESDIS Sea Surface Temperature Estimation Technique in the Oceans around Japan." *Journal of Oceanography* 48: 345–351.

Takikawa, T., J.-H. Yoon, and K.-D. Cho. 2005. "The Tsushima Warm Current through Tsushima Straits Estimated from Ferryboat ADCP Data." *Journal of Physical Oceanography* 35: 1154–1168.

Talley, L. D., V. Lobanov, V. Ponomarev, A. Salyuk, P. Tishchenko, and I. Zhabin. 2003. "Deep Convection and Brine Rejection in the Japan Sea." *Geophysical Research Letter* 30 (4): 1159. doi:10.1029/2002GL016451.

Van Loon, H. 1967. "The Half-Yearly Oscillations in Middle and High Southern Latitudes and the Coreless Winter." *Journal of Atmospheric Science* 24: 472–486.

Walton, C. C., W. G. Pichel, J. F. Sapper, and D. A. May. 1998. "The Development and Operational Application of Nonlinear Algorithms for the Measurement of Sea Surface Temperatures with the NOAA Polar-Orbiting Environmental Satellites." *Journal of Geophysical Research* 103 (C12): 27999–28012.

Wyrtki, K. 1965. "The Annual and Semiannual Variation of Sea Surface Temperature in the North Pacific Ocean." *Limnology and Oceanography* 10 (3): 307–313.

Xie, S., J. Hafner, Y. Tanimoto, W. T. Liu, H. Tokinaga, and H. Xu. 2002. "Bathymetric Effect on the Winter Sea Surface Temperature and Climate of the Yellow and East China Seas." *Geophysical Research Letter* 29 (24): 2228. doi:10.1029/2002GL015884.

Yan, X.-H., J. R. Shubel, and D. W. Pritchard. 1990. "Oceanic Upper Mixed Depth Determination by the Use of Satellite Data." *Remote Sensing Environment* 32: 55–74.

Yashayaev, I. M., and I. I. Zveryaev. 2001. "Climate of the Seasonal Cycle in the North Pacific and the North Atlantic Oceans." *International Journal of Climatology* 21: 401–417.

Yoon, J. H. 1982. "Numerical Experiment on the Circulation in the Japan Sea, Part II. Influence of Seasonal Variations in Atmospheric Conditions on the Tsushima Current." *Journal of the Oceanographical Society of Japan* 38: 43–51.